PERGAMON

International Journal of Solids and Structures 39 (2002) 2059–2085

INTERNATIONAL JOURNAL OF SOLIDS and STRUCTURES

www.elsevier.com/locate/ijsolstr

Bending instabilities of elastic tubes

Spyros A. Karamanos *

Department of Mechanical and Industrial Engineering, University of Thessaly, 38334 Volos, Greece

Received 25 November 2001; received in revised form 8 December 2001

Abstract

The present paper examines instabilities of long thin elastic tubes. Both initially straight and initially bent tubes are analyzed under in-plane bending. Tube response, a combination of ovalization instability and bifurcation instability (buckling), is investigated using a nonlinear finite element (FE) technique, which employs polynomial functions in the longitudinal tube direction and trigonometric functions to describe cross-sectional deformation. It is demonstrated that the interaction between the two instability modes depends on the value and the sign of the initial tube curvature. The ovalization of initially bent tubes is examined in detail and, in particular, the case of opening moments. Furthermore, the paper emphasizes on bifurcation instability. It is shown that buckling may occur prior to or beyond the ovalization limit point, depending on the value of the initial curvature. Using the nonlinear FE formulation, the location of bifurcation on the primary path is detected, post-buckling equilibrium paths are traced, and the corresponding wavelengths of the buckled configurations are calculated. Moreover, results over a wide range of initial curvature values are presented, extending the findings of previous works. Finally, several analytical approaches, introduced in previous research works, are also employed to estimate the moments causing ovalization and bifurcation instability. These approaches are based on nonlinear flexible shell theory or simplified ring analysis. The efficiency and accuracy of those analytical methods with respect to the nonlinear FE formulation are examined.

Keywords: Tube; Pipe bend; Stability; Ovalization; Buckling; Post-buckling; Bifurcation

1. Introduction and literature review

The main characteristic of a tube under bending is the distortion (ovalization) of its cross-section (Fig. 1a) because of the inward stress components σ_v (Fig. 1b). The ovalizing mechanism results in loss of stiffness in the form of limit point instability, referred to as "ovalization instability". Furthermore, the increased axial stress at the compression side due to ovalization may cause bifurcation instability (buckling) in a form of longitudinal wavy-type "wrinkles" usually before a limit moment is reached (Fig. 1a).

In the present paper, ovalization and bifurcation instabilities of thin elastic tubes are examined (Fig. 2). The tubes considered herein are thin, with cross-sectional radius-to-thickness ratio (r/t) greater than 100,

* Tel.: +30-4210-74086; fax: +30-4210-74009.
E-mail address: skara@mie.uth.gr (S.A. Karamanos).

0020-7683/02/$ - see front matter
PII: S0020-7683(02)00085-9

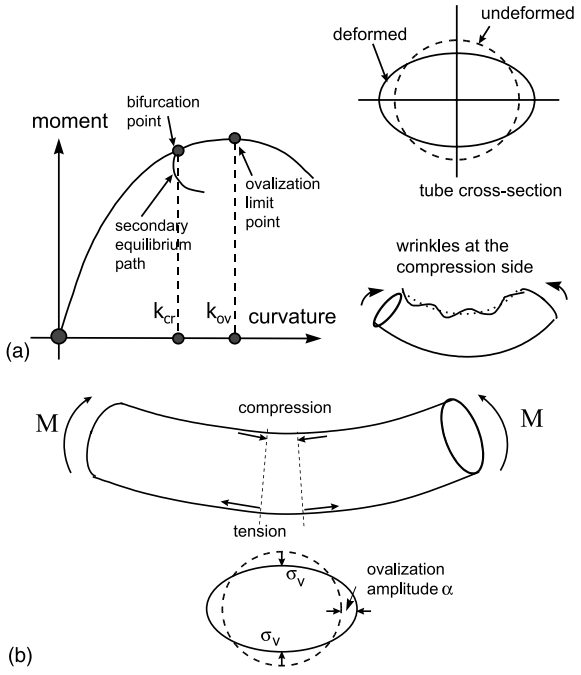

Fig. 1. Schematic representation of (a) ovalization vs. bifurcation instability and (b) ovalization mechanism, because of inward stress components σ_v.

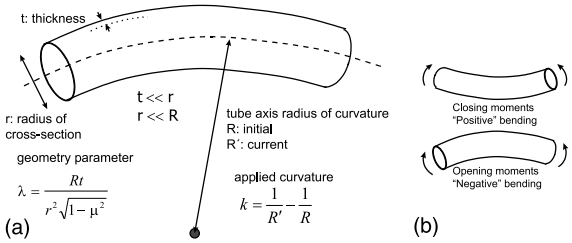

Fig. 2. (a) Tube geometry and (b) loading conditions in initially bent tubes.

and exhibit elastic response (plasticity effects are not considered). The tubes may be initially straight or initially bent with a longitudinal radius of curvature R significantly larger than the cross-sectional radius r ($R/r > 80$). The following parameter is employed to describe tube geometry:

$$\lambda = \frac{Rt}{r^2\sqrt{1-\mu^2}} \tag{1}$$

where t is the tube thickness and is the Poisson's ratio (Fig. 2). Tubes may be subjected to closing moments (''positive'' bending) or opening moments (''negative'' bending) as shown in Fig. 2. The present work is based on a nonlinear finite element (FE) formulation. Using this numerical formulation, it is possible to investigate issues, which were not examined in previous works. Among other results, values of buckling

wavelength are reported in terms of initial curvature, and the nature of post-buckling paths and the post-buckling configurations are examined in detail. Furthermore, the FE results are compared with those obtained from simplified methods introduced in previous publications.

1.1. Ovalization instability

An early study of elastic elbow ovalization under in-plane bending (von Karman, 1911), assumed inextentional cross-section and neglecting nonlinear terms. A Rayleigh–Ritz method was adopted in terms of doubly symmetric trigonometric functions for the cross-sectional displacements, resulting in a linear relationship between the ovalization and the applied curvature, as a function of the geometric parameter Rt/r^2. This pioneering work was extended by several researchers towards the analysis of pipes and elbows, as well as the development of design formulae for flexibility and stress concentrations. Among others, Vigness (1943), Beskin (1945), Pardue and Vigness (1951), Gross (1952), Gross and Ford (1952), Rodabough and George (1957) extended the work by von Karman to investigate out-of-plane bending response of curved tubes (especially short-radius elbows) and the effects of pressure. The analytical results were supported by experimental evidence. The flexibility factors and the stress concentration factors proposed by those works constitute the basis of current specifications for pipe and elbow design.

Clark and Reissner (1951) reformulated the problem of curved pipe linear bending in terms of two independent variables, the rotation of the ring (β) and a stress function (ψ), resulting in two differential equations, solved through the use of trigonometric series. Cheng and Thailer (1970) reexamined the linear bending of elbows investigating the effects of λ on the response. Sobel (1977) also studied the linear bending response of elbows comparing previous analytical results with the results from two computer programs (ELBOW and MARC), and presented interesting results for tube flexibility and stresses intensity factors. Bathe and Almeida (1980) proposed a simple and efficient elbow element for the linear analysis of curved piping components, assuming a cubic interpolation of displacement, rotation and ovalization parameters along the tube.

The nonlinear bending response of initially straight tubes (i.e. $1/R = 0$) was studied by Brazier (1927). The work was based on a variational formulation, which considers both longitudinal and inextensional circumferential (ovalization) deformation. Using simple nonlinear kinematics and assuming isotropic elastic material, Brazier obtained a doubly symmetric trigonometric solution for the cross-sectional displacement function and a quadratic expression of the ovalization, in terms of the applied curvature. The ultimate moment and the corresponding curvature were found equal to:

$$M_{\mathrm{BR}} = 0.987\frac{Ert^2}{\sqrt{1-\mu^2}} \quad \text{and} \quad k_{\mathrm{BR}} = 0.471\frac{t}{r^2\sqrt{1-\mu^2}} \tag{2}$$

for tube flattening equal to about 22% of the tube diameter (E is the Young's modulus). Wood (1958) examined the ovalization instability of initially straight tubes using a variational formulation, including external pressure effects. Cross-sectional deformation was considered inextensional, discretized through a trigonometric series (Fourier) expansion.

Reissner (1959) was the first to investigate ovalization instability of initially straight and initially curved tubes from a unified point-of-view considering nonlinear ring kinematics, including the effects of pressure. Furthermore, Reissner (1961) examined in detail the ovalization instability of initially straight tubes, considering two independent variables, namely the rotation of the cross-section reference line $\beta(\theta)$, and a stress function $\psi(\theta)$, where θ is the hoop coordinate. For circular cross-section, the formulation resulted in a system of two nonlinear differential equations in terms of β and ψ. The moment–curvature (M–k) path, included terms up to the fifth power of the curvature, improving the third-degree expression of Brazier. In a subsequent paper, Reissner and Weinitschke (1963) presented an integral formulation for the ovalization

instability of circular initial straight tubes and an iterative numerical solution method. Results for deformation and stress beyond the limit point were reported.

Axelrad (1961, 1962) presented a nonlinear formulation for the ovalization instability of tubular members under bending based on a nonlinear flexible shell theory. Results were reported for initially straight and bent tubes, including the effects of pressure. For initially straight tubes, the formulation is identical to the one developed by Reissner (1961). A description of this formulation and some characteristic results can be found in Axelrad (1980, 1987) and in Axelrad and Emmerling (1984). In a later publication of Emmerling (1981) a Fourier series solution of the governing equations was presented. Thurston (1977) used a modified Newton's method to solve the governing equations proposed by Reissner (1961) and calculated the ultimate moment and the corresponding curvature due to ovalization instability of initially straight tubes. Those values correlate very well with the analytical results presented by Axelrad (1962, 1980). Boyle (1981) re-examined the instability of initially bent tubes under in-plane bending, considering a similar nonlinear shell theory. The solution was compared with simplified closed-form M–k expressions, and was in very good agreement with the results of Axelrad (1962).

More recently, several works on ovalization instability have been presented, motivated by the instability problems of offshore pipelines. A nonlinear semi-analytical formulation of the ovalization instability of relatively thick elastoplastic tubes under bending and external pressure was proposed by Kyriakides and Shaw (1982), based on an inextensional nonlinear ring theory (Brush and Almroth, 1975), assuming moderate hoop curvature changes, in terms of single-symmetric trigonometric functions. Subsequently, Shaw and Kyriakides (1985) and Corona and Kyriakides (1988) improved the formulation relaxing the inextensionality condition and allowing for large changes of hoop curvature. The analytical results were compared with experimental data from small-scale tests. In a more recent work, Karamanos and Tassoulas (1991) investigated ovalization instability of initially straight relatively thick tubes using nine-node degenerated shell elements, and kinematic constraints to enforce uniform ovalization along the tube. The results compared very well with the experimental and analytical results for thick tubes reported by Corona and Kyriakides (1988).

1.2. Bifurcation instability

Bifurcation instability of tubes under bending (Fig. 1a), often referred to as "buckling", was recognized in early publications (Brazier, 1927). An attempt to predict the bending buckling of tubes was reported by Seide and Weingarten (1961) assuming a wavy post-buckling shape, through trigonometric shape functions. The formulation did not consider the cross-sectional deformation (ovalization) effects on the pre-buckling state. Therefore, the results can be used for calculating the buckling moment of short tubes with restrained ends and predicted unrealistic critical moments for long tubes free to ovalize. Furthermore, Seide and Weingarten concluded that the buckling moment of a cylinder under bending corresponds to a nominal stress quite similar to the buckling stress of a cylinder with the same radius under uniform compression. Using this approximate concept of "axially uniformly compressed cylinder", Chen and Kempner (1976) have examined the buckling response of oval cylinders under bending and thrust. The Donnell shell equations were employed to determine the state of stress, and the local curvature around the oval cross-section was considered. However, the buckling load was computed on the basis of the undeformed configuration and the pre-buckling distortion (ovalization) of the cylinder was neglected.

An important contribution towards considering the effects of the ovalized (deformed) pre-buckling configuration was introduced by Axelrad (1965), through the so-called "local buckling hypothesis" (LBH): bifurcation is determined by the situation inside the initial (localized) buckle zone. Therefore, buckling is assumed to occur when the maximum compressive stress reaches the uniform compression critical value for

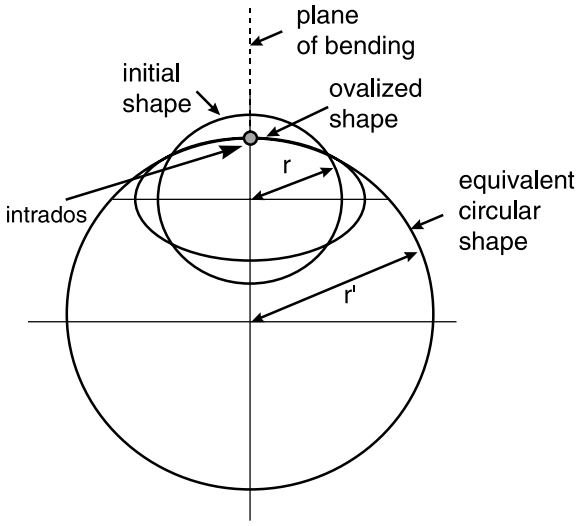

Fig. 3. Simplified assumption for estimating bifurcation instability.

a circular tube of radius equal to the local radius of the ovalized shell at the "critical" point. This critical point is usually the extreme fiber of the compression zone ($\theta = \pi/2$ "intrados" (Fig. 3)). Axelrad (1987) describes an asymptotic analysis, which supports the LBH. This concept was a major improvement of the concept of Chen and Kempner (1976), and buckling moments for initially straight and bent tubes were obtained. Emmerling (1982) applied this concept to initially oval cylinders under pressure. An extensive presentation of those results can also be found in Axelrad (1980, 1987), Axelrad and Emmerling (1983, 1984).

Stephens et al. (1975) investigated bifurcation buckling of straight tubes, based on a nonlinear shell analysis through a finite-difference technique. Bifurcation moments were calculated assuming a slight initial imperfection, pre-buckling ovalization was taken into account and the sensitivity of buckling on the level of pressure and the boundary conditions was also investigated. It was observed that for unpressurized long tubes (boundary conditions free), buckling occurs before a limit moment is reached. Fabian (1977) examined the buckling behavior of thin elastic initially straight tubes under bending and external pressure, through an energy approach and a perturbation analysis, employing the Donnell–Mushtari–Vlasov shallow shell equations. Results showed that the buckling point occurs before the ovalization limit point. A similar methodology was adopted by Gellin (1980) who investigated both ovalization and bifurcation instability of thin elastic tubes under bending.

Ju and Kyriakides (1992) presented an alternative formulation for the analysis of initially straight tubes under bending, with emphasis on the buckling of relatively thick inelastic tubes, through Sander's nonlinear shell theory. Trigonometric shape functions were used in both the longitudinal and the hoop direction. Both types of instability were examined and a good comparison with experimental data was found. Few cases of thin elastic tubes ($r/t = 100$) in terms of bifurcation instability were examined, verifying that buckling occurs before a limit point is reached.

In more recent works, Karamanos and Tassoulas (1996a, 1996b) developed a nonlinear three-node "tube element" capable of describing cross-sectional deformation. Both bifurcation and ovalization instabilities were investigated mainly for thick inelastic tubes, candidates for offshore applications. Few results for elastic initially straight tubes under bending were also reported and verified that bifurcation occurs before

the tube reaches the ovalization limit moment. The numerical formulation developed in those papers is used as a basis for the present study.

2. Finite element formulation

A nonlinear FE formulation is adopted, which has been used successfully for predicting the ultimate capacity of thick inelastic tubes under the combined action of thrust, moment and pressure (Karamanos and Tassoulas, 1996a, 1996b). Herein, thin tubes, which exhibit only elastic deformations, are considered. The formulation is based on a Lagrangian description of the tube, including geometric nonlinearities. Convected coordinates are considered in the hoop, longitudinal and radial direction (denoted as θ, ζ, ρ respectively). The material is isotropic hypo-elastic, the constitutive equations relate the convected rate of Kirchhoff stress to the rate-of-deformation tensor, and the instantaneous moduli are evaluated at the deformed configuration. Following classical shell theory, the traction component normal to any shell lamina is imposed to be zero. Equivalently, the stress component along the radial coordinate is imposed equal to zero throughout the deformation. Details on the formulation can be found in Karamanos and Tassoulas (1996a).

2.1. Discretization—tube element

The tube element combines longitudinal (beam-type) with cross-sectional deformation (ovalization). Isoparametric beam FE concept is used to describe longitudinal deformation, with three nodes defined along the tube axis (Fig. 4). Geometry and displacements are interpolated using quadratic polynomials. Bending is applied about axis x_1 (i.e. x_2–x_3 is the plane of bending) and each node possesses three DOFs (two translational and one rotational), which define its position and orientation. The deformed tube axis is defined by

$$\mathbf{x}_c(\zeta) = \sum_{k=1}^{3} N^{(k)}(\zeta)\mathbf{x}^{(k)} \tag{3}$$

where $\mathbf{x}^{(k)}$ is the position vector of node (k) and $N^{(k)}(\zeta)$ is the corresponding Lagrangian quadratic interpolation function. To describe cross-sectional deformation, thickness is assumed to be constant and a

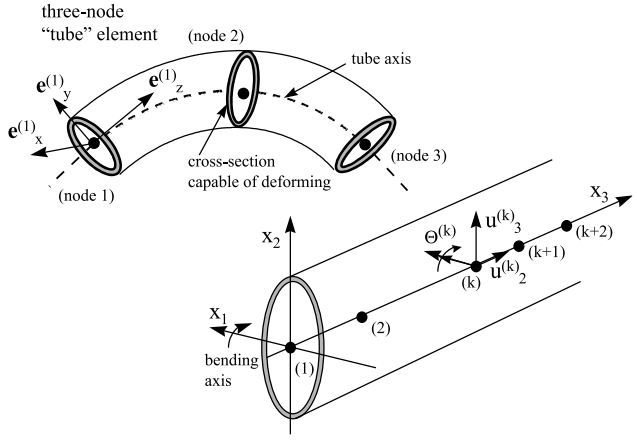

Fig. 4. Tube element; x_2–x_3 is the plane of bending.

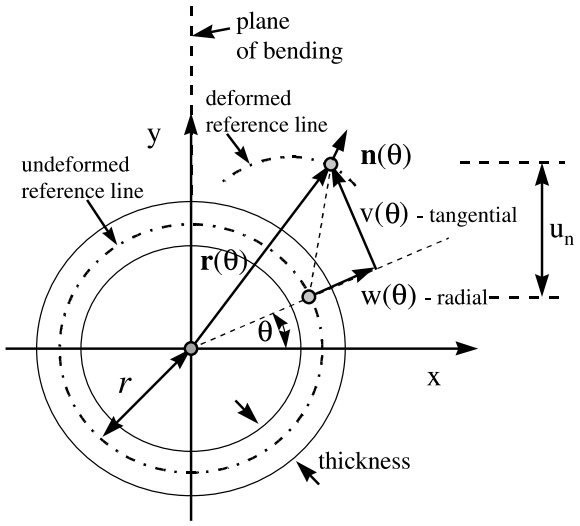

Fig. 5. Cross-sectional ovalization (in-plane) deformation parameters.

reference line is chosen within the cross-section. Both in-plane and out-of-plane (warping) cross-sectional deformation are considered, defined by the orthonormal vectors $\mathbf{e}_x^{(k)}$, $\mathbf{e}_y^{(k)}$, $\mathbf{e}_z^{(k)}$. For in-plane deformation, fibers initially normal to the reference line remain normal to the reference line. The position of the reference line at the cross-section corresponding to node (k) is

$$\mathbf{r}^{(k)}(\theta) = x_r(\theta)\mathbf{e}_x^{(k)} + y_r(\theta)\mathbf{e}_y^{(k)} + z_r(\theta)\mathbf{e}_z^{(k)} \tag{4}$$

where

$$\begin{aligned} x_r(\theta) &= [r + w(\theta)]\cos\theta - v(\theta)\sin\theta \\ y_r(\theta) &= [r + w(\theta)]\sin\theta + v(\theta)\cos\theta \\ z_r(\theta) &= u(\theta) \end{aligned} \tag{5}$$

are the components of $\mathbf{r}^{(k)}(\theta)$ with respect to the cross-section vector triplet (Fig. 5). In the above expressions, $w(\theta)$, $v(\theta)$ and $u(\theta)$ are displacements of the reference line in the radial, tangential and out-of-plane (axial) direction respectively. The material fibers normal to the reference line may rotate in the out-of-plane direction by angle $\gamma(\theta)$ so that the position vector of an arbitrary point at the deformed configuration is

$$\mathbf{x}(\vartheta, \zeta, \rho) = \sum_{k=1}^{3} \left[(\mathbf{x}^{(k)} + \mathbf{r}^{(k)}(\theta) + \rho\mathbf{n}^{(k)}(\theta) + \rho\gamma(\theta)\mathbf{e}_z^{(k)}) N^{(k)}(\zeta) \right] \tag{6}$$

where $\mathbf{n}^{(k)}(\theta)$ is the "in-plane" outward normal of the reference line at the deformed configuration:

$$\mathbf{n}^{(k)}(\theta) = \left(-\frac{1}{r}\frac{\mathrm{d}y_r}{\mathrm{d}\theta} \right)\mathbf{e}_x^{(k)} + \left(\frac{1}{r}\frac{\mathrm{d}x_r}{\mathrm{d}\theta} \right)\mathbf{e}_y^{(k)} \tag{7}$$

For an extensive presentation of ring analysis, the reader is referred to the book by Brush and Almroth (1975). The deformation functions $w(\theta)$, $v(\theta)$, $u(\theta)$ and $\gamma(\theta)$ are discretized as follows:

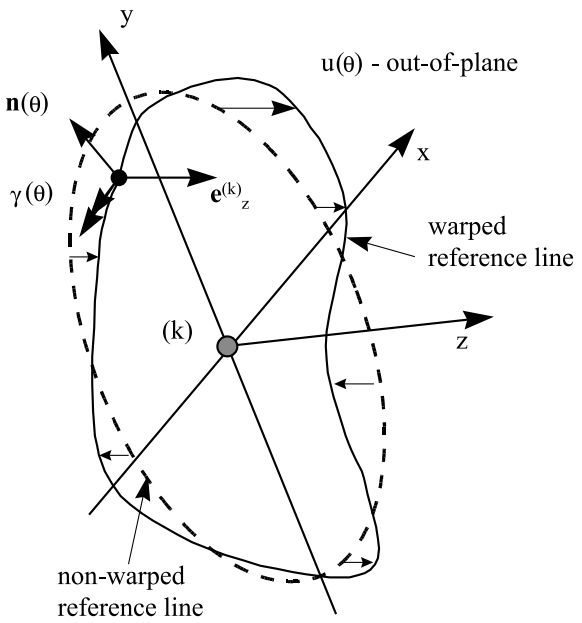

Fig. 6. Cross-sectional warping (out-of-plane) deformation parameters.

$$
\begin{aligned}
w(\theta) &= a_0 + a_1 \sin\theta + \sum_{n=2,4,6,\ldots} a_n \cos n\theta + \sum_{n=3,5,7,\ldots} a_n \sin n\theta \\
v(\theta) &= -a_1 \sin\theta + \sum_{n=2,4,6,\ldots} b_n \sin n\theta + \sum_{n=3,5,7,\ldots} b_n \cos n\theta \\
u(\theta) &= \sum_{n=2,4,6,\ldots} c_n \cos n\theta + \sum_{n=3,5,7,\ldots} c_n \sin n\theta \\
\gamma(\theta) &= \gamma_0 + \gamma_1 \sin\theta + \sum_{n=2,4,6,\ldots} \gamma_n \cos n\theta + \sum_{n=3,5,7,\ldots} \gamma_n \sin n\theta
\end{aligned}
\tag{8}
$$

Coefficients a_n, b_n refer to in-plane cross-sectional deformation (“ovalization” parameters, Fig. 5) and c_n, γ_n refer to out-of-plane cross-sectional deformation (“warping” parameters, Fig. 6). In the above expressions, symmetry with respect to the x_2–x_3 plane is considered because of in-plane bending and only half of the tube is analyzed ($-\pi/2 \leqslant \theta \leqslant \pi/2$).

2.2. Issues of numerical implementation

In the general case (three-dimensional analysis) both in-plane and out-of-plane deformations are considered for ovalization analysis only, a cross-sectional (two-dimensional) analysis is conducted, restraining out-of-plane deformation parameters. To analyze bifurcation instability, a three-dimensional analysis is necessary, and details are presented in Section 4.2.

Numerical results from previous works (Karamanos and Tassoulas, 1996b), indicated that the post-buckling path may be highly unstable, possibly exhibiting “snap back”. In order to trace the path, the arc-length algorithm was employed (Crisfield, 1983), which monitors the value of the so-called “arc-length” parameter. This is a combination of the moment increment with the increment of some “selected” degrees

of freedom $\Delta\mathbf{u}$. In the present analysis the incremental nodal displacements $\Delta u_2^{(k)}$ and $\Delta u_3^{(k)}$ (see Fig. 4) are used in vector $\Delta\mathbf{u}$.

A preliminary parametric study is conducted, to examine the number of cross-sectional parameters to be used, and a 14th degree expansion ($n \leqslant 14$ in Eq. (8)) for $w(\theta)$, $v(\theta)$, $u(\theta)$ and $\gamma(\theta)$ is found to be adequate for the cases of interest. Regarding the number of integration points in the circumferential direction, the 14th degree expansion requires 19 equally spaced integration points around the half-circumference including the two points on the symmetry plane. Five and two Gauss points are used in the radial (through the thickness) direction and the longitudinal direction respectively.

3. Simple formulation and solution for ovalization instability

To investigate ovalization instability, cross-sectional analysis is required. Therefore, only displacements $w(\theta)$ and $v(\theta)$ are taken into account, and no variation along the tube is considered. Since the pioneering works by von Karman (1911) and Brazier (1927), numerous researchers have examined bending of tubes, refining the formulation. The following simple energy formulation developed in various forms elsewhere (e.g. Vigness (1943), Rodabough and George (1957), for linear elbow analysis and Wood (1958), Cheng and Thailer (1970), Calladine (1983) for ovalization instability) is presented herein from a unified point-of-view, to clarify some special issues which are discussed in Section 4.

3.1. Strain energy formulation

The total strain energy U per unit length of the tube, consists of a "longitudinal" and a "hoop" part, because of longitudinal (beam-type) and cross-sectional deformation respectively:

$$U = U_{\mathrm{L}} + U_{\mathrm{C}} \tag{9}$$

From beam theory, the longitudinal part U_{L} is expressed in terms of the stress (σ_{L}) and the strain (ε_{L}) in the direction of tube axis as follows:

$$U_{\mathrm{L}} = \frac{1}{2}\int_A \sigma_{\mathrm{L}}\varepsilon_{\mathrm{L}}\,\mathrm{d}A = \frac{E}{2}\int_A \varepsilon_{\mathrm{L}}^2\,\mathrm{d}A = \frac{Etr}{2}\int_0^{2\pi} \varepsilon_{\mathrm{L}}^2\,\mathrm{d}\theta \tag{10}$$

The strain ε_{L} in the direction of the tube axis is

$$\varepsilon_{\mathrm{L}} = ky + \frac{u_n}{R} = k[(r+w)\sin\theta + v\cos\theta] + \frac{1}{R}[v\cos\theta + w\sin\theta] \tag{11}$$

where $1/R = k_{\mathrm{i}}$ is the initial curvature of the tube, r and t are the radius and the thickness of the tube cross-section respectively, y is the distance from the neutral axis, u_n is the displacement in the direction of the plane of bending (see Fig. 5), and k is the longitudinally applied curvature. The first part of the right-hand-side of Eq. (11) comes from beam theory, and the second part corresponds to the longitudinal strain due to u_n. The total curvature $1/R'$ is

$$\frac{1}{R'} = k + \frac{1}{R} \tag{12}$$

Referring to the hoop strain energy U_{C}, a curved-beam formulation is adopted, based on the Bernoulli assumption (plane sections remain plane). Every point has an axial hoop strain (Brush and Almroth, 1975):

$$\varepsilon_\theta = \varepsilon_{\theta 0} + k_\theta\rho = \left[\frac{1}{r}\left(v' + w\right)\right] + \left[\frac{1}{r^2}\left(v' - w''\right)\right]\rho \tag{13}$$

where $(\,)'$ denotes differentiation with respect to θ, ρ is the material coordinate in the radial direction (through the thickness), $\varepsilon_{\theta 0}$ is the mean axial strain of the mid surface, t is the tube thickness and k_θ is the change of curvature in the hoop direction. If inextentionality of the tube perimeter is assumed, $\varepsilon_{\theta 0}$ is equal to zero

$$\varepsilon_{\theta 0} = 0 \quad \Longleftrightarrow \quad w + \frac{\mathrm{d}v}{\mathrm{d}\theta} = w + v' = 0 \tag{14}$$

The expression for the hoop strain energy U_C using Eqs. (13) and (14) can be expressed as follows

$$U_C = \frac{1}{2}\int\int_{A_\theta} \sigma_\theta \varepsilon_\theta r \,\mathrm{d}\theta\,\mathrm{d}\rho = \frac{1}{2}\frac{Er}{(1-\mu^2)}\int\int_{A_\theta} \varepsilon_\theta^2 \,\mathrm{d}\theta\,\mathrm{d}\rho = \frac{Et^3}{24(1-\mu^2)r^3}\int_0^{2\pi} (v' + v''')\mathrm{d}\theta \tag{15}$$

3.2. Rayleigh–Ritz solution

It is possible to obtain analytical closed-form solutions (ovalization–curvature ζ–κ relationship and the moment–curvature equilibrium path) through a Ritz discretization in terms of trigonometric functions. Assuming only one trigonometric doubly symmetric term for $w(\theta)$ and $v(\theta)$:

$$w(\theta) = \alpha \cos 2\theta \quad \text{and} \quad v(\theta) = -\frac{\alpha}{2}\sin 2\theta \tag{16}$$

where α is the ovalization amplitude. Note that the above deformation is inextensional (Eq. (14)) and can be considered as a special case of Eq. (8) for $w(\theta)$ and $v(\theta)$ ($n = 2$, $a_2 = -2b_2$). Inserting Eq. (16) in the expression of tube energy, U becomes:

$$U = \frac{Etr}{2}\left(k^2 r^2 \pi + \frac{5a^2}{8R'^2}\pi - \frac{3}{2}\frac{kra}{R'}\pi\right) + \frac{3}{8}\frac{\pi E t^3 a^2}{(1-\mu^2)r^3} \tag{17}$$

Solutions for the ovalization parameter α in terms of the applied curvature k yield directly from the minimization of U in terms of α. Subsequently, using this expression, differentiation of U in terms of k yields the M–k equilibrium path.

Using the above discretization, it is possible to obtain simplified solutions for initially straight and curved tubes, and various assumptions and simplifications. In Table 1 (Panel A), solutions are presented in

Table 1
ζ–κ and M–k relationships (Panel A) from Eq. (17) and (Panel B) for initially bent tubes

	Ovalization–curvature	Moment–curvature	
Panel A			
Brazier (1927) initially straight	$\zeta = \kappa^2$	$m = \pi\kappa\left[1 - \frac{3}{2}\kappa^2\right]$	(A)
Modified Brazier initially straight	$\zeta = \kappa^2 \frac{1}{1+\frac{5\kappa^2}{6}}$	$m = \pi\kappa\left[1 - \frac{3}{2}\zeta + \frac{5}{8}\zeta^2\right]$	(B)
von Karman (1911) initially bent	$\zeta = \frac{\kappa\lambda}{\lambda^2+\frac{5}{6}}$	$m = \pi\kappa\left[1 - \frac{9}{10+12\lambda^2}\right]$	(C)
Modified von Karman initially bent	$\zeta = \frac{\kappa\lambda(1+\kappa\lambda)}{\lambda^2+\frac{5}{6}(1+\kappa\lambda)^2}$	$m = \pi\kappa\left[1 - \frac{3}{4}\zeta\left(2+\frac{1}{\kappa\lambda}\right) + \frac{5}{8}\zeta^2\left(1+\frac{1}{\kappa\lambda}\right)\right]$	(D)
Panel B			
Reissner (1959)	$\zeta = \frac{\kappa\lambda}{\lambda^2} + \kappa^2$	$m = \pi\kappa\left[1 - \frac{3}{4\lambda^2}(1+\kappa\lambda)(1+2\kappa\lambda)\right]$	(E)
Boyle (1981)		$m = \frac{\pi\kappa)}{(1-\mu^2)} + \left[1 - \frac{3}{4\lambda^2}\frac{(1+\kappa\lambda)(1+2\kappa\lambda)}{(1-\mu^2)+\frac{5(1+\kappa\lambda)^2}{6\lambda^2}}\right]$	(F)

a dimensionless form. The values of moment M and all curvature values $(k, k_i, 1/R')$ are normalized by M_e and k_N respectively, where

$$M_e = \frac{Ert^2}{\sqrt{1-\mu^2}} \quad \text{and} \quad k_N = \frac{t}{r^2\sqrt{1-\mu^2}} \tag{18}$$

so that

$$m = M/M_e \quad \text{and} \quad \kappa = k/k_N \tag{19}$$

are the normalized moment and the normalized applied curvature respectively. Furthermore, the value of the ovalization amplitude is normalized by the tube radius r, so that $\zeta = \alpha/r$. Note that the normalized initial curvature ($\kappa_i = k_i/k_N$) of a tube is equal to $1/\lambda$.

Eqs. (A) (in Table 1) refer to initially straight tubes ($\lambda = \infty$, $k_i = 1/R = 0$), neglect higher order terms, and are identical to those derived by Brazier (1927). The derivation of Eqs. (A) (in Table 1) from the strain energy is also described by Calladine (1983). Eqs. (B) (in Table 1) also refer to initially straight tubes but consider all terms of expression (17). Eqs. (C) (in Table 1) refer to initially curved tubes but consider only linear terms (von Karman solution). Finally, Eqs. (B) (in Table 1) refer to initially curved tubes considering all terms of Eq. (17). More details for the derivation of Eqs. (A–D) (in Table 1) are reported in Karamanos (2000). For comparison purposes, two other closed-form solutions (E) and (F) reported by Reissner (1959) and Boyle (1981) are presented in Table 1 (Panel B). The analytical ovalization results presented by Axelrad (1962, 1980), Axelrad and Emmerling (1983) and Boyle (1981) are considered in Section 4.

4. Numerical results

Numerical FE results are obtained for thin elastic tubes for both ovalization instability and bifurcation instability. The material is elastic (plasticity effects are not considered), with Young's modulus E and Poisson ratio μ equal to 29,000 ksi and 0.3 respectively. Values of moment, curvature and ovalization are normalized by M_e, k_N and r respectively (see Eqs. (17) and (18)). Results are obtained for tubes with r/t equal to 120. Nevertheless, using the above normalization values, identical results are obtained for elastic tubes of different r/t ratio. Ovalization instability is considered first, under the assumption that bifurcation (buckling) may not occur. Subsequently, bifurcation is examined, taking into account the ovalized pre-buckling configuration. Numerical FE results are compared with results from analytical solutions.

4.1. Ovalization (limit moment) instability

In Fig. 7a and b the FE results (from a cross-sectional two-dimensional analysis) for initially straight tubes are compared with simplified equations (A) and (B) (in Table 1) in the absence of bifurcation. The comparison shows that those simplified equations cannot predict accurately the response, but can be used for a qualitative interpretation of ovalization instability. The results show that Fourier coefficient a_0, the uniform expansion/contraction term in Eq. (8), has monotonically decreasing negative value and, therefore, tube "flattening" develops faster than tube "bulging" (Fig. 8). Therefore, inextensional assumed shape functions, satisfying Eq. (16), may not provide accurate results for large deformation stages.

Initially bent tubes are also analyzed, with κ_i ranging from 0 to ± 1.4, so that the corresponding initial radius R is large in comparison with the cross-sectional radius r ($R/r > 80$). Moreover, the applied curvature at which ovalization instability occurs (κ_{ov}) is of the same order of magnitude with the initial curvature ($|\kappa_i| = 1/\lambda$). Negative κ_i value means that the initial curvature is opposite to the direction of bending (opening moments or negative bending). Equilibrium paths (m–κ) obtained from the rigorous

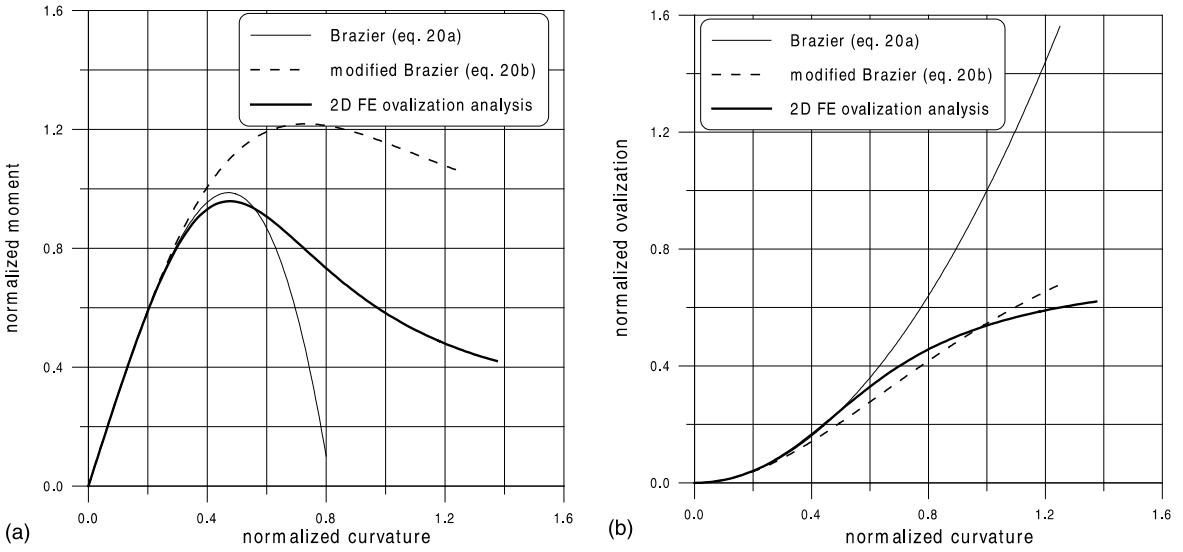

Fig. 7. Ovalization analysis of initially straight tubes ($\kappa_i = 0$, $\lambda = \infty$) (a) m–κ path; (b) ζ–κ relationship; FE ovalization analysis compared with simplified closed-form solutions.

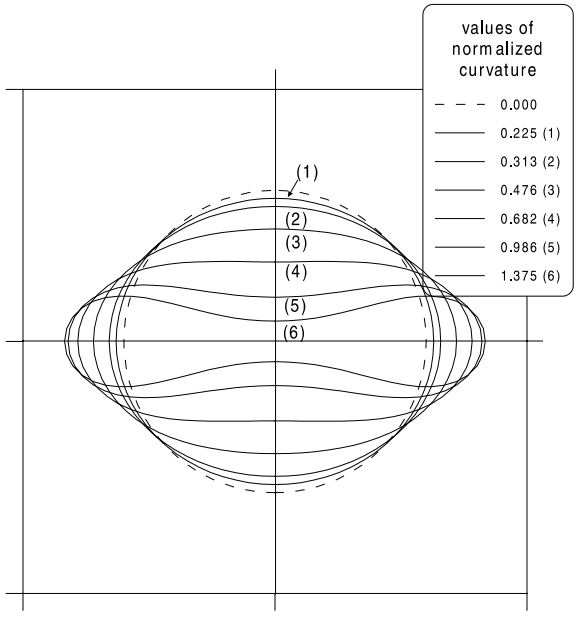

Fig. 8. Ovalization analysis of initially straight tubes; cross-sectional configurations for different values of applied curvature; FE analysis in the absence of bifurcation (no amplification factor).

technique are shown in Fig. 9 for $\kappa_i = 0, \pm 0.343$. Closing moments result in significant ovalization and a "smooth" limit point. The ultimate moment is reduced when the value of the initial curvature is increased. For opening moments, the response is characterized by smaller deformations, and a significantly higher

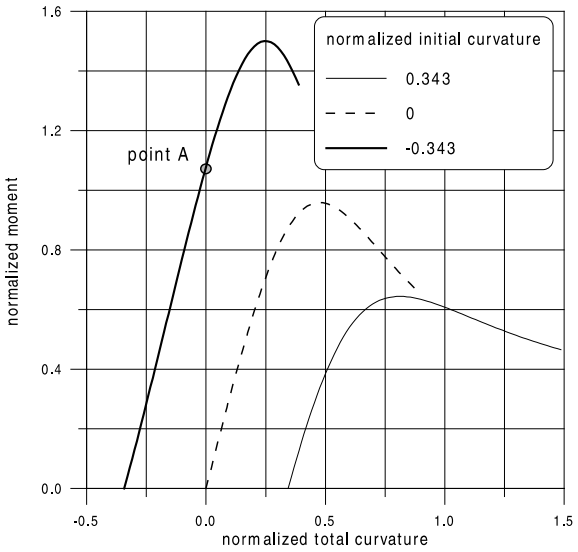

Fig. 9. Ovalization analysis of initially bent tubes; m–κ paths; opening and closing moments, no bifurcation. At point A, the tube under opening moments becomes straight.

limit moment and a "sharper" ovalization limit point. The different m–κ response between the opening moment and the closing moment cases was also recognized in the work of Axelrad (1961, 1962, 1987). FE results for initially bent tubes are compared with simplified solutions (D), (E) and (F) (in Table 1) in Fig. 10a and b. The comparison indicates that those simplified closed-form solutions do not provide a good estimate of the ultimate moment (due to the inextensionality condition) but can be used for qualitative purposes. On the other hand, the present FE results fall very close to the thin shell analytical solution of Boyle (1981), as shown in Fig. 10c, and the analytical results reported by Axelrad (1980), Emmerling (1981) and Axelrad and Emmerling (1983) in Fig. 10d.

The ζ–κ relationship for different values of initial curvature κ_i under opening moments is depicted in Fig. 11. In such a case, the direction of the stress components σ_v in the vertical y–y direction is outward. It is therefore expected that the response under opening moments is quite different than the response under closing moments. More specifically it is expected that negative ovalization occurs, so that the tube diameter on the bending plane (D_v) elongates and that the other diameter (D_h), about which bending is applied, shortens. It is further expected that negative ovalization would continue to increase up to the point that the applied curvature eliminates the initial curvature, i.e. the tube becomes straight ($\kappa = |\kappa_i|,\ \sigma_v = 0$), and that, immediately after this point, the tube would start to ovalize in the opposite direction, because the stress components σ_v become inward.

However, FE ζ–κ solutions of Fig. 11 for tubes of different initial curvature under negative bending do not verify the latter argument. The total normalized curvature is considered in the horizontal axis (the algebraic sum of κ_i and κ). Initially, the vertical diameter increases and the horizontal diameter shortens (negative ovalization). On the other hand, this behavior occurs until the total curvature becomes about half the initial curvature value ($\kappa \approx |\kappa_i|/2$). Beyond this stage, ovalization decreases and becomes zero at the point where the tube becomes straight ($\kappa = |\kappa_i|$).

The above imply that for κ values between $|\kappa_i|/2$ and $|\kappa_i|$, the tube ovalizes in a direction opposite to the direction of the corresponding stress components σ_v. To interpret those results, the Reissner solution (Eqs. (A) (in Table 1)) is considered. The ζ–κ relationship consists of two parts, a linear and a quadratic part. When ($\kappa_i < 0$) the linear term (similar to von Karman solution) causes tube flattening in the y–y axis

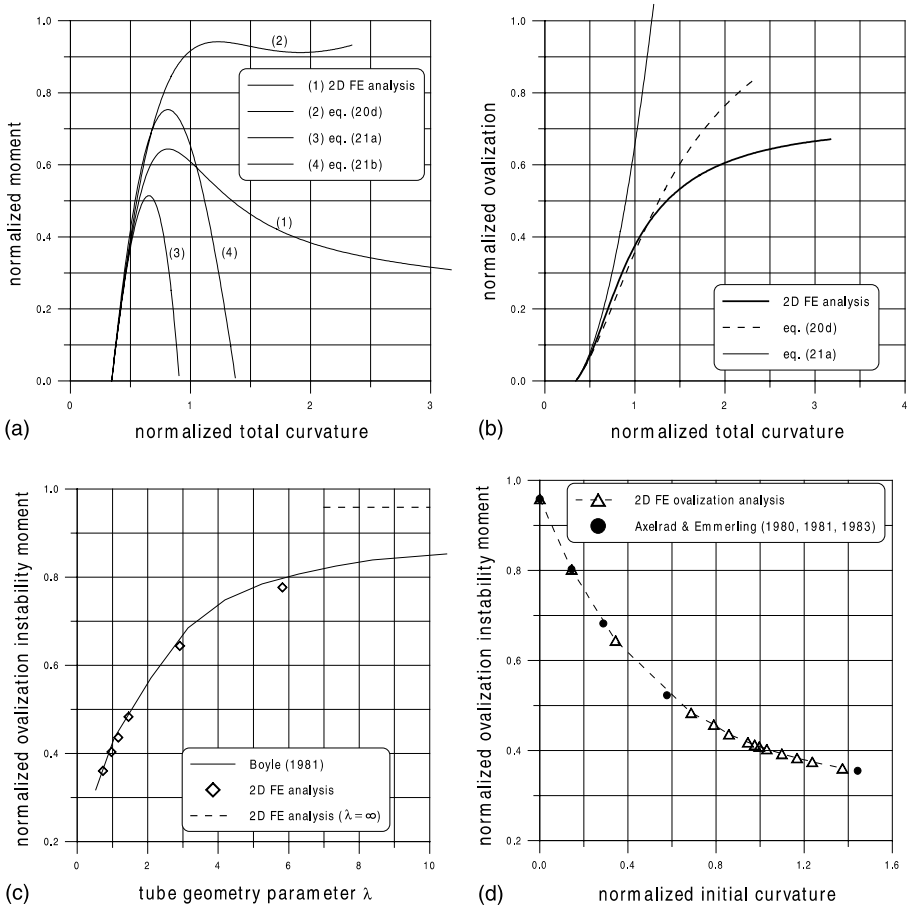

Fig. 10. FE ovalization (2D) analysis versus analytical solutions for initially curved tubes (closing moments): (a) m–κ path, simplified solutions ($\kappa_i = 0.343$, $\lambda = 2.912$); (b) ζ–κ relationship, simplified solutions ($\kappa_i = 0.343$); (c) ultimate moments, Boyle (1981) and (d) ultimate moments, Axelrad (1980), Emmerling (1981), Axelrad and Emmerling (1983).

(negative ovalization) and the nonlinear term (Brazier) causes flattening in the x–x direction (normal to the plane of bending). The latter is independent of the value and the sign of κ_i. In case of opening moments, the two parts "counteract". For small values of κ, the linear term is more dominant so that negative ovalization occurs. However, the Brazier effect grows fast (in a quadratic rate) and results in a reversal of ovalization at $\kappa = |\kappa_i|/2$. Similar conclusions can be extracted using Eq. (D) (in Table 1). It is reminded that the results are obtained under the assumption of absence of bifurcation.

Two additional observations are made, for opening moments and for the stage where the applied curvature "eliminates" the initial curvature ($\kappa = |\kappa_i|$)

1. The moment is equal to the moment required for straightening a tube ignoring any cross-sectional deformation (see point A in Fig. 9). This has been observed first by Axelrad (1962, 1987).
2. The ovalization is zero, so that in Fig. 11 all curves pass through the origin. This implies that ovalization becomes zero when the tube becomes straight for all values of initial curvature. Eq. (D) and Reissner equations (E) (in Table 1) support this argument.

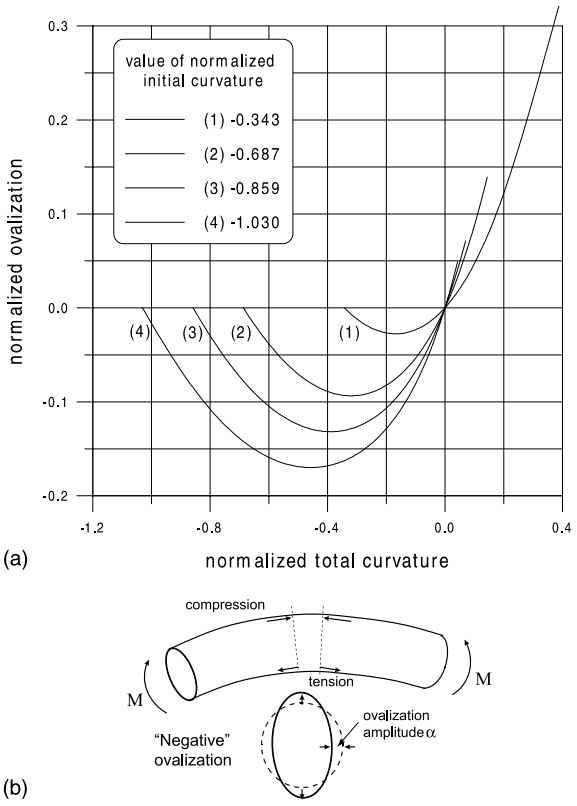

Fig. 11. (a) Ovalization analysis of initially bent tubes; ζ–κ relationships for different values of initial curvature; opening moment (''negative'' bending); FE numerical results and (b) negative ovalization mechanism under opening moments, because of outward stress components σ_v.

4.2. Bifurcation instability—numerical implementation and results

Beyond the buckling point, cross-sectional deformation is no longer constant along the tube (due to the developed wrinkles). Therefore, a three-dimensional analysis is necessary, so that warping deformation and its variation along the tube need to be accounted for, through the warping parameters c_n, γ_n of the ''tube'' element.

In a wavy-type post-buckling configuration (formation of wrinkles) of an infinitely long tube, cross-sections A–A and B–B (Fig. 12a) do not exhibit warping deformation for symmetry reasons. Thus, for the purposes of our analysis, it is sufficient to analyze only a tube segment of half wavelength (i.e. from A to B). Warping parameters (c_n and γ_n) at ''end-sections'' A and B are set equal to zero because of symmetry. The wavelength is not known a priori and, therefore, a sequence of analyses should be conducted for several assumed wavelength values. The actual wavelength is the one that corresponds to the ''earliest'' bifurcation point on the primary path. Ju and Kyriakides (1992) and Karamanos and Tassoulas (1996b) used a similar methodology to analyze initially straight tubes. Results from those papers for initially straight tubes showed that the half wavelength L_{hw} normalized by $(Dt)^{1/2}$ ($l_{hw} = L_{hw}/(Dt)^{1/2}$) is equal to about 1.7. This value is used herein as an initial (trial) value of l_{hw}. Regarding the number of elements in the longitudinal direction, four elements per half wavelength are employed.

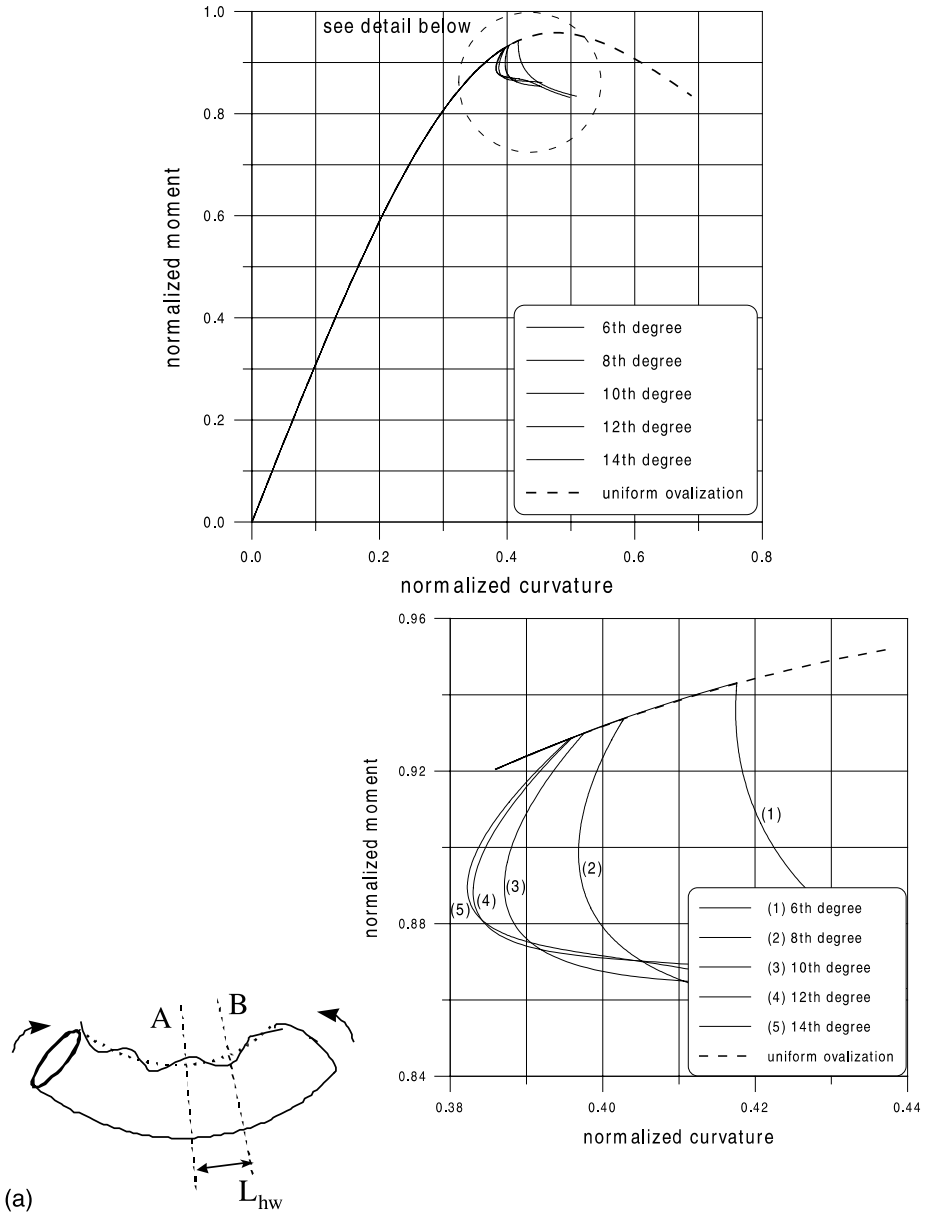

Fig. 12. Bifurcation analysis of initially straight tubes; (a) m–κ paths; effect of the degree of trigonometric expansion; FE numerical results; $m_{cr} = 0.929$, $\kappa_{cr} = 0.396$, (b) cross-sections of the buckled configuration (post-buckling displacements are magnified and shapes are distorted).

Prior to buckling, cross-sectional deformation is almost doubly symmetric. Upon buckling, the development of wrinkles on the compression side would result the cross-section configuration looses its symmetry with respect to the x–x axis. Parameter a_1 is the first nondoubly symmetric Fourier term. Thus, the a_1 value is expected to increase significantly when bifurcation occurs. The amplitude of this imperfection is

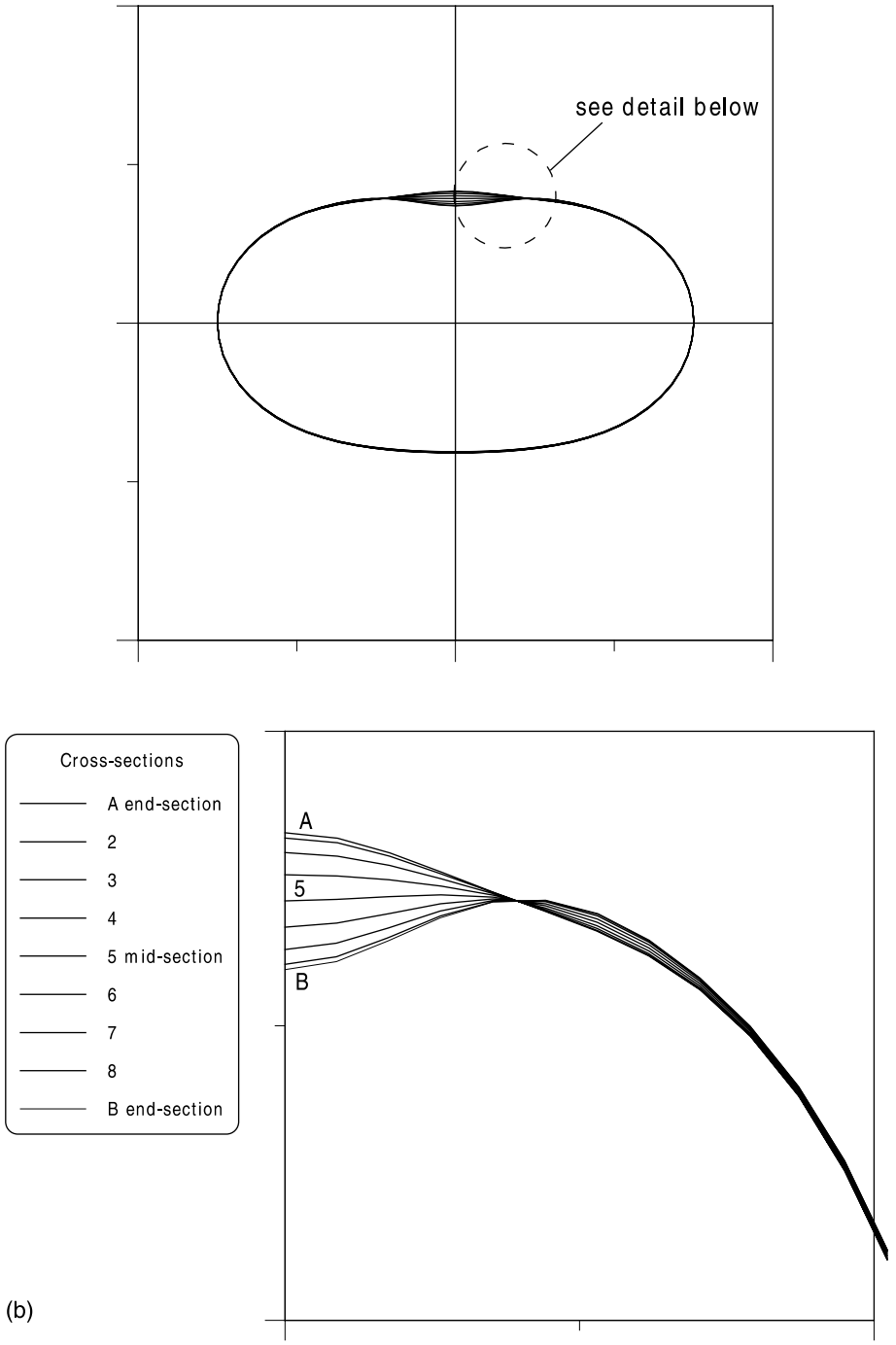

Fig. 12 (*continued*)

assumed equal to 10^{-8} times the tube radius, very small yet sufficient to "trigger" bifurcation and to enable the tube to follow the secondary (post-buckling) path.

Table 2
Bifurcation points (values of m_{cr} and κ_{cr}) for different assumed values of wavelength; initially straight tube ($r/t = 120$)

Normalized half wavelength $l_{hw} = L_{hw}/(Dt)^{1/2}$	Normalized critical moment m_{cr}	Normalized curvature at which buckling occurs κ_{cr}
1.5	0.9343	0.4036
1.6	0.9302	0.3980
1.7	0.9286	0.3957
1.75	0.9284	0.3955
1.8	0.9285	0.3957
1.9	0.9295	0.3969

Results from an initially straight tube are depicted in Fig. 12a and summarized in Table 2 for different assumed values of l_{hw}. A "snap-back" immediately after bifurcation characterizes the post-buckling path, which is reminiscent of the equilibrium path of axially uniformly compressed tubes (e.g. Hutchinson, 1968). Bifurcation occurs at $m_{cr} = 0.9284$ and $\kappa_{cr} = 0.3955$, i.e. before ovalization instability ($\kappa_{cr}/\kappa_{ov} = 0.83$), and corresponds to $l_{hw} = 1.75$. Table 2 also indicates that the critical moment and the corresponding curvature are not sensitive to substantial changes of l_{hw}. For a 23% variation on the assumed value of l_{hw}, m_{cr} changes only by 0.5% and κ_{cr} by 1.75%. The shape of nine equally spaced cross-sections along the half wavelength of the buckled configuration are shown in Fig. 12b. They correspond to a deformation stage immediately after bifurcation. In that figure, the post-buckling displacements are magnified and, therefore, the depicted shapes are distorted with respect to the actual shapes. Differences between the consecutive cross-sections, which are responsible for a wavy-type post-buckling deformation, occur within a part of the compression zone around the intrados.

Initially curved tubes are also examined in terms of buckling. Fig. 13 shows the results for a tube with $\lambda = 2.912$ ($\kappa_i = 0.343$, $R/r = 333.3$) under positive bending (closing moments). Buckling occurs before the limit point ($\kappa_{cr}/\kappa_{ov} = 0.892$). The post-buckling path is also characterized by a "snap-back", less pronounced than the initially straight tube, is equal to 2.2. Fig. 14 shows the bifurcation instability of a tube

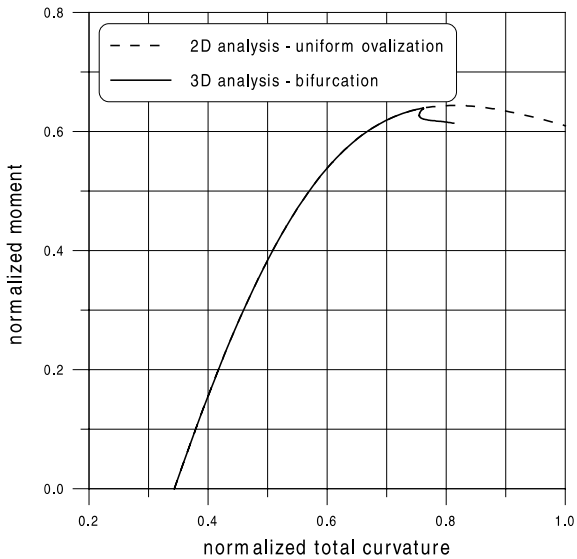

Fig. 13. Bifurcation analysis of initially bent tube ($\kappa_i = 0.343$, $\lambda = 2.912$); m–κ path for closing moments (positive bending); comparison with ovalization analysis path.

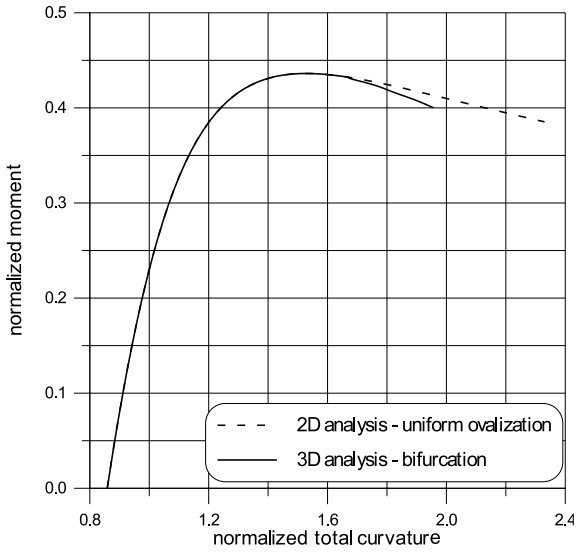

Fig. 14. Bifurcation analysis of initially bent tube ($\kappa_i = 0.858$, $\lambda = 1.165$); m–κ path for closing moments (positive bending); comparison with ovalization analysis path.

with $\lambda = 1.165$ ($\kappa_i = 0.858$, $R/r = 133.3$) under closing moments. Bifurcation occurs significantly after the limit point ($\kappa_{cr}/\kappa_{ov} = 1.212$) and l_{hw} is equal to 4.05. The post-buckling path is unstable and characterized by a less pronounced snap back.

The results for the above two tubes under opening moments ($\lambda = -2.912/\kappa_i = -0.343$, and $\lambda = -0.728$ $\kappa_i = -1.374$) are shown in Figs. 15 and 16. The negative values of λ denote bending in a direction opposite

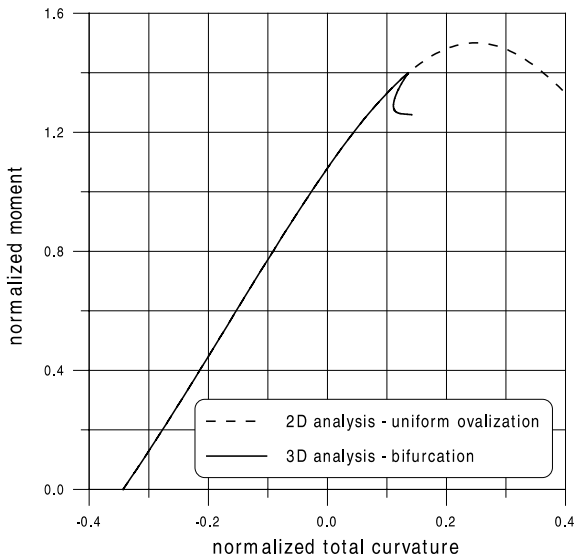

Fig. 15. Bifurcation analysis of initially bent tube ($\kappa_i = -0.343$, $\lambda = -2.917$); m–κ path for opening moments (negative bending); comparison with ovalization analysis path.

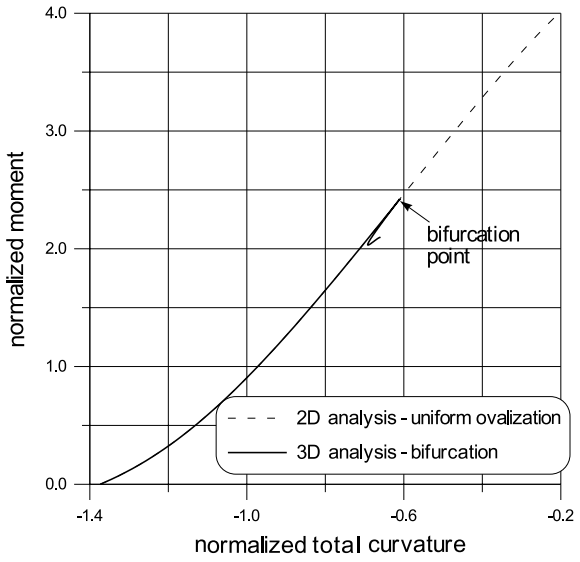

Fig. 16. Bifurcation analysis of initially bent tube ($\kappa_i = -1.374$, $\lambda = -0.728$); m–κ path for opening moments (negative bending); comparison with ovalization analysis path.

to the initial curvature. In both cases, bifurcation occurs before limit point. The post-buckling path is characterized by a sharp snap back and l_{hw} is equal to 1.45 and 1.65 respectively. For the first case (Fig. 15) buckling occurs after the tube becomes straight (total curvature equal to zero), whereas for the second case (Fig. 16), buckling occurs prior to this point.

4.3. Bifurcation instability—simplified approach

It is possible to use a more simplified analytical approach to estimate the location of bifurcation on the primary (ovalization) path, by applying the so-called LBH (Axelrad, 1965) on the pre-buckling distorted (ovalized) cross-sectional configuration. In circular tubes under uniform axial compression σ_u, linear stability analysis yields the following buckling stress (Timoshenko and Gere, 1961):

$$\sigma_{u,cr} = \frac{1}{\sqrt{3(1-\mu^2)}}\left(E\frac{t}{r}\right) \simeq 0.6E\frac{t}{r} \tag{20}$$

The latter equation assumes $\mu = 0.3$ and is extensively used in thin shell design. Following LBH, and in order to take into account the ovalized pre-buckling shape, it is assumed that a tube under bending buckles when the stress at the critical point becomes equal to $0.6Et/r'$, where $1/r'$ is the local curvature of tube circumference. This critical point is usually assumed to be the point with the maximum compressive strain (intrados, $\theta = \pi/2$, for relatively small κ_i values (Axelrad, 1980). If the ovalization solution is known, the value of the local curvature at the critical point is determined (see Eq. (13)):

$$\frac{1}{r'} = \frac{1}{r} + k_\theta = \frac{1}{r} + \frac{1}{r^2}(v' - w'') \tag{21}$$

In the course of a nonlinear step-by-step ovalization analysis, the bifurcation point on the ovalization (primary) path is obtained by monitoring at each step the values of stress and local curvature at the critical

point (Eq. (20)). Using this approach, the tube is approximated with a uniformly compressed circular tube of radius r'.

It is possible to extend the above concept to estimate the buckling half wavelength from the corresponding formula of axially uniformly compressed tubes (Timoshenko and Gere, 1961), but using the local radius r' instead of r

$$L'_{\mathrm{hw}} = \pi\left(\frac{1}{12(1-\mu^2)}\right)^{1/4}\sqrt{r't} \tag{22}$$

In the present work, LBH is applied first on the FE ovalization (two-dimensional) solution at the intrados point. For initially straight tubes ($\kappa_{\mathrm{i}} = 0$, $\lambda = \infty$), it estimates a buckling moment $m'_{\mathrm{cr}} = 0.9215$, a corresponding curvature $\kappa'_{\mathrm{cr}} = 0.386$ and a normalized half wavelength $l'_{\mathrm{hw}} = L'_{\mathrm{hw}}/(Dt)^{1/2} = 1.63$, which are very close to the three-dimensional FE values m_{cr}, κ_{cr} and l_{hw} (see Table 2). Emmerling (1982) has applied LBH on his analytical solution for ovalization instability, and obtained a critical normalized moment value 0.922, almost identical to m_{cr}, m'_{cr}.

4.4. Discussion

The FE results imply that buckling and post-buckling are strongly affected by the value of initial curvature. In case of initially straight tubes (Fig. 12) and for initially bent tubes under opening moments (Figs. 15 and 16), buckling occurs always before ovalization instability and the secondary path is characterized by a significant "snap back". On the other hand, for closing moments (positive bending), buckling may occur prior to the limit point for $\kappa_{\mathrm{i}} \leqslant 0.68$ (Fig. 13) or beyond the limit point for $\kappa_{\mathrm{i}} \geqslant 0.68$ (Fig. 14). When the κ_{i} value is greater than about 0.9, the post-buckling path tends to "follow" the primary path and bifurcation becomes less significant. In other words, for opening moments, bifurcation instability governs the response, whereas for closing moments the ovalization mechanism is generally more dominant.

In Fig. 17a and b, the critical values of moment m_{cr} and of the applied curvature κ_{cr}, obtained from a three-dimensional FE analysis, are plotted in terms of κ_{i}. The same figures also show the critical values m'_{cr} and κ'_{cr} obtained from the application of LBH on the FE ovalization path (two-dimensional analysis) assuming that $\theta = \pi/2$ is the critical point. This assumption seems reasonable, taken into account that the κ_{i} values are relatively small ($R/r > 80$). The figures also show the results of Emmerling (1982), which are also based on LBH and concern tubes with $\kappa_{\mathrm{i}} \leqslant 0.80$. In Fig. 18 the normalized half wavelength calculated through a three-dimensional FE analysis (l_{hw}), and that from the simplified approach ($l'_{\mathrm{hw}} = L'_{\mathrm{hw}}/(Dt)^{1/2}$) are plotted in terms of κ_{i}.

Figs. 17 and 18 show that the above application of the LBH concept provides remarkably good results for $-1 \leqslant \kappa_{\mathrm{i}} \leqslant 0.95$. However, there are significant deviations outside this range. In Fig. 17b, the κ'_{cr} values seem to grow very rapidly for $\kappa_{\mathrm{i}} \geqslant 0.95$. This might imply that, when $\kappa_{\mathrm{i}} \geqslant 0.95$, bifurcation occurs at very large curvature values. However, this is not verified by the three-dimensional FE results and, thus, it requires some further investigation. Similar observation is made for the l'_{hw} value when $\kappa_{\mathrm{i}} \geqslant 0.95$ in Fig. 18. To clarify the above observation, it is reminded that in curved tubes under bending, the intrados does not correspond to the maximum longitudinal stress point. In Fig. 19, longitudinal stresses are shown for a tube with $\kappa_{\mathrm{i}} = 1.030/\lambda = 0.971$ under closing moments, at the ovalization instability stage and just before bifurcation. The stresses are obtained from a two-dimensional FE ovalization analysis (negative stress means compression) and are normalized by

$$\sigma_{\mathrm{e}} = \frac{E}{\pi\sqrt{1-\mu^2}}\left(\frac{t}{r}\right) \tag{23}$$

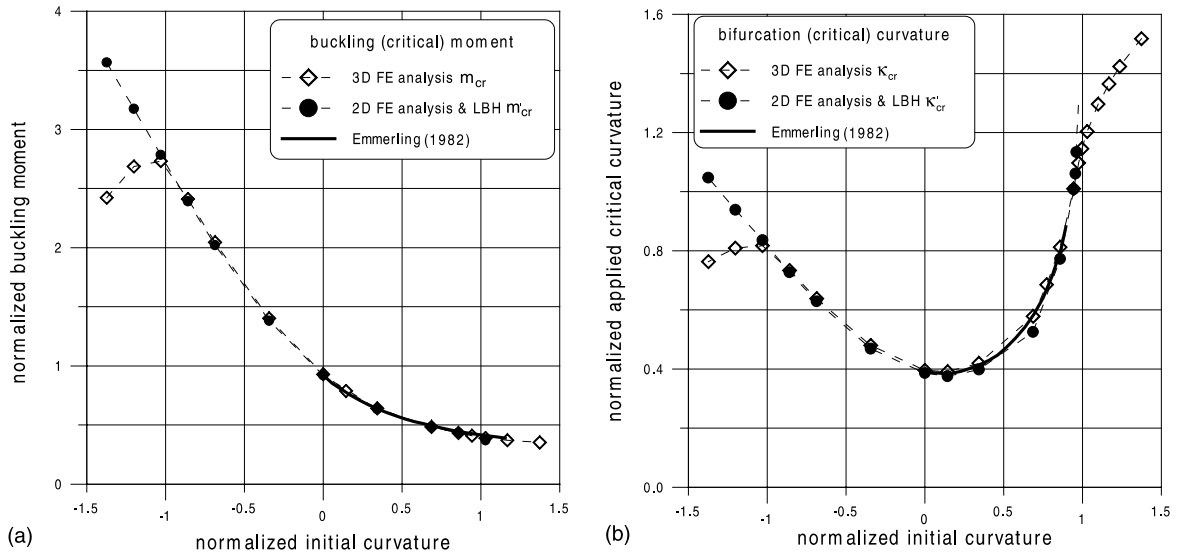

Fig. 17. (a) Buckling moments and (b) curvature at which bifurcation occurs in terms of the initial curvature. LBH is applied at the $\theta = \pi/2$ location.

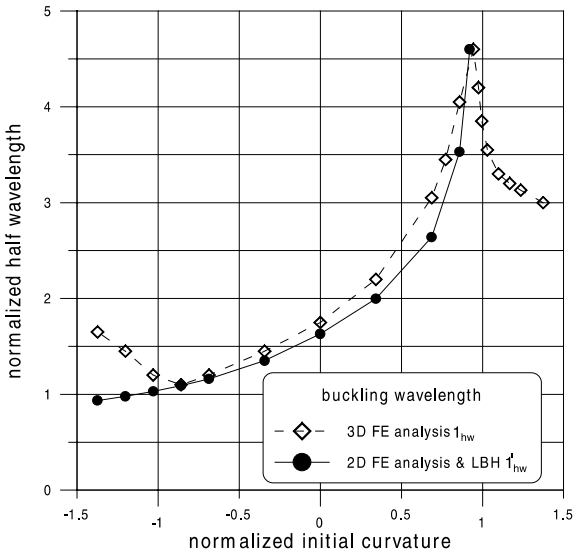

Fig. 18. Wavelength of the post-buckling configuration in terms of the initial curvature. LBH is applied at the $\theta = \pi/2$ location.

At bifurcation, the stress at the intrados ($\theta = \pi/2$) has already become tensile (positive) and, therefore, this point is by no means critical in terms of buckling. For the case considered, the LBH concept (Eqs. (20) and (21)) is applied to each one of the 12 equally spaced points around the tube (compression zone): stresses and local curvatures are monitored at each one of those points, at each step of the ovalization analysis. When Eqs. (20) and (21) are satisfied at a certain point, a possible bifurcation location on the primary path is determined. The critical point is the point where bifurcation occurs earlier. In the present case, point no. 4

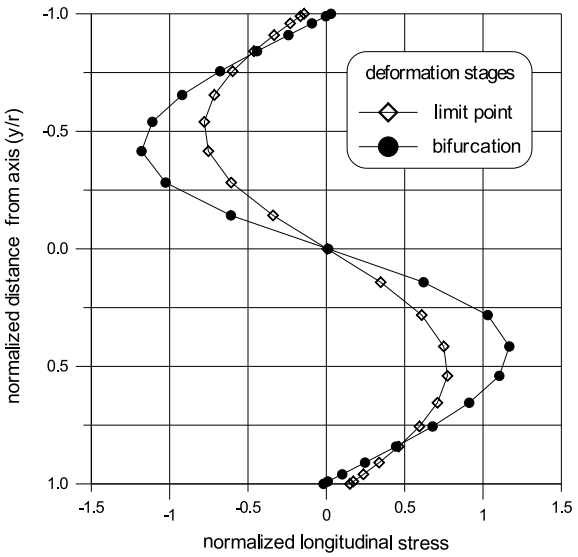

Fig. 19. Longitudinal stress distribution of an initially bent tube ($\kappa_i = 1.030$, $\lambda = 0.971$) under closing moments the ovalization limit point stage and at the bifurcation point.

($\theta = 65.6°$) is critical, and corresponds to $\kappa'_{cr} = 1.46$, which is comparable to the FE prediction ($\kappa_{cr} = 1.20$), as shown in Fig. 20. Application of the same methodology in other cases with closing moments shows that, when κ_i is greater than about 0.95, $\theta = \pi/2$ is no longer critical in terms of buckling. This explains the differences between the three-dimensional numerical results and those obtained from the application of LBH on the ovalization path (two-dimensional analysis) in Figs. 17a,b and 18.

For the case of opening moments, the maximum stress at the bifurcation point is located at $\theta = \pi/2$, as shown in Fig. 21 for an initially curved tube ($\lambda = -0.728$). However, the minimum local curvature $1/r'$ point is not located at $\theta = \pi/2$ (Fig. 22a). The LBH criterion is applied to each one of the 12 equally spaced points around the tube. Fig. 22b indicates that the critical point is no. 8 ($\theta = 32.7°$), which is far away from the intrados. The corresponding bifurcation location on the primary path is quite close to the FE result.

The above results indicate that the application of LBH at the intrados provides accurate results over a certain range of initial curvatures ($-1 \leqslant \kappa_i \leqslant 0.95$). Out of this range, a more refined analysis is necessary. More specifically, Eqs. (20) and (21) can be used in a "more elaborate" manner to obtain accurate results: after obtaining an accurate ovalization (cross-sectional) solution, all points around the cross-section (not only the intrados) should be considered to determine the critical point and to predict bifurcation. This methodology offers good results compared with three-dimensional nonlinear FE analysis.

5. Conclusions

Results from a nonlinear FE analysis verify the observation of previous researchers that the ultimate capacity of elastic thin tubes under in-plane bending depends on two instability modes (ovalization and bifurcation), which interact each other strongly. It is also demonstrated that even small values of initial tube curvature have very significant effects on tube response. Furthermore, the paper presents some new results on bifurcation and post-buckling response of tubes.

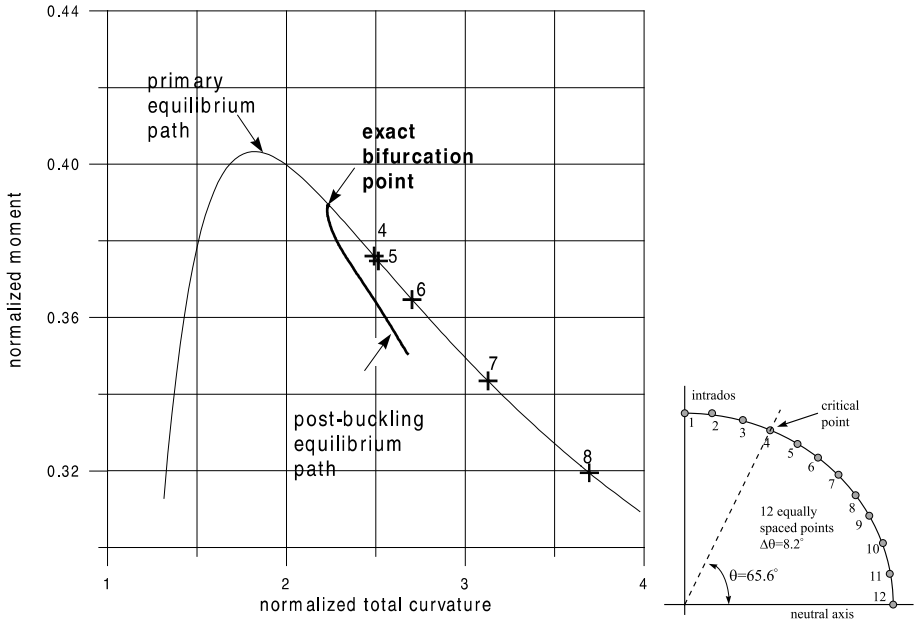

Fig. 20. Bifurcation buckling of a tube ($\kappa_i = 1.030$, $\lambda = 0.971$) under opening moments; buckling predictions applying LBH (Eqs. (20) and (21)) at 12 equally spaced points.

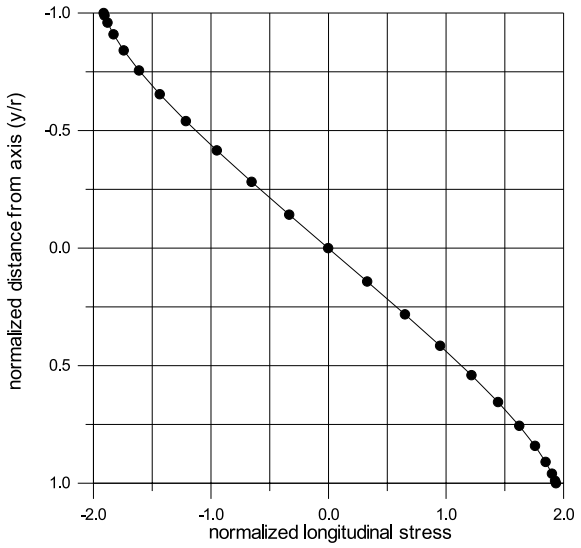

Fig. 21. Longitudinal stress distribution of an initially bent tube ($\kappa_i = -1.374$, $\lambda = -0.728$) under opening moments at the bifurcation point.

The analysis employs a nonlinear "tube" FE, which uses polynomial functions in the longitudinal tube direction and trigonometric functions to describe cross-sectional deformation. Trigonometric functions up

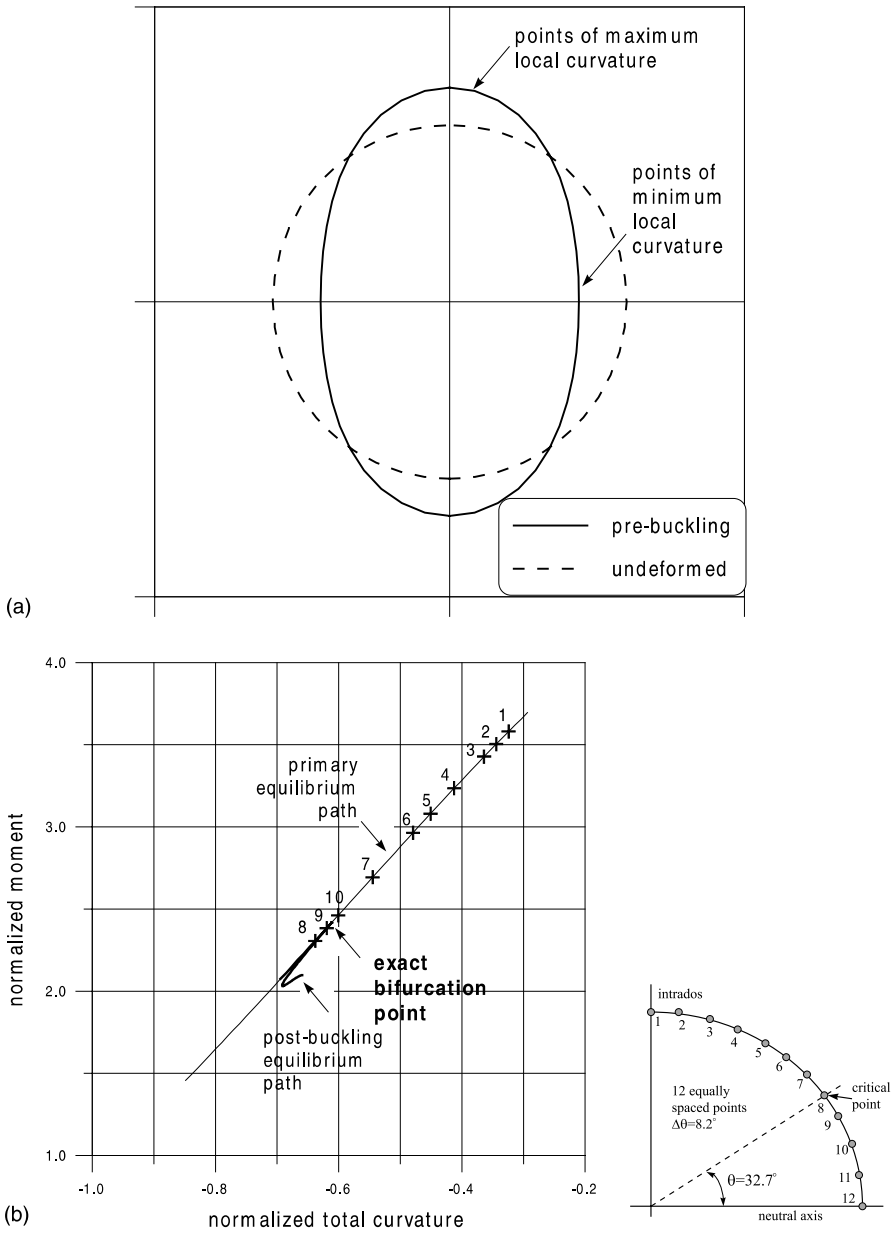

Fig. 22. Bifurcation buckling of a tube ($\kappa_i = -1.374$, $\lambda = -0.728$) under opening moments: (a) cross-sectional shape at the bifurcation stage; (b) buckling predictions applying LBH (Eqs. (20) and (21)) at 12 equally spaced points.

to 14th-degree, and a path-follower algorithm to trace snap-back paths are necessary for the purposes of obtaining unstable post-buckling paths.

Cross-sectional ovalization is examined first, in the absence of bifurcation. This type of deformation has an immediate effect on the moment capacity and changes the local curvature around the tube significantly. A very good comparison is obtained between the FE ovalization results and previous ovalization results

from nonlinear flexible shell analysis. In particular, tube ovalization under opening moments is examined, and the phenomenon of negative ovalization is investigated in detail. The FE results, as well as those from simplified analytical solutions, show that the ovalization solution of initially bent tubes can be considered as a sum of a linear (von Karman) part and a quadratic (''Brazier'') part. It is also demonstrated that the nonlinear (quadratic) part of the ovalization solution is rather independent of the initial curvature κ_i and causes always positive ovalization (i.e. tube flattening normal to the plane of bending).

Bifurcation instability (buckling) occurs in the form of ''wrinkles'' and is generally characterized by an unstable post-buckling path, which indicates sudden collapse. For initially straight tubes, buckling occurs prior to ovalization instability. Bifurcation is followed by a snap back of the post-buckling (secondary) equilibrium path. The presence of initial curvature in the direction of bending (closing moments) makes the ovalization mechanism more dominant, and results in bifurcation beyond ovalization instability ($\kappa_{cr} \geqslant \kappa_{ov}$), for $\kappa_i \geqslant 0.68$. Furthermore, for κ_i greater than about 0.9 bifurcation instability effects become less significant and the post-buckling path is close to the primary path. On the other hand, opening moments cause less ovalization, bifurcation is ''sharp'', it is followed by a very pronounced snap back and it occurs always prior to the ovalization limit point.

A more simplified analytical method (based on the so-called LBH), introduced elsewhere, is also employed to locate the bifurcation point on the primary equilibrium (ovalization) path. When applied at the tube intrados and for a certain range of initial curvature values ($-1 \leqslant \kappa_i \leqslant 0.95$), the method (despite its simplicity) provides remarkably good results (in terms of buckling moment, curvature and wavelength) in comparison with the nonlinear FE results. Outside this range, the method may not provide accurate results if applied at the intrados point only, because this point may not be critical in terms of buckling. A more elaborate application of this method for initially bent tubes is suggested to obtain improved bifurcation instability predictions, which are in good agreement with the three-dimensional FE results.

Acknowledgements

The author would like to thank Professor John L. Tassoulas (The University of Texas at Austin) for his comments and suggestions.

References

Axelrad, E.L., 1961. Flexure of thin-walled beams under large elastic displacements. Izvestiya Akademii Nauk SSSR, Otdelenie Tekhnicheskikh Nauk, Mekhanika i Mashinostroenie 3, 124–132, in Russian.

Axelrad, E.L., 1962. Flexure and instability of thin-walled pressurized tubes. Izvestiya Akademii Nauk SSSR, Otdelenie Tekhnicheskikh Nauk, Mekhanika i Mashinostroenie 1, 98–114, in Russian.

Axelrad, E.L., 1965. Refinement of buckling-load analysis for tube flexure by way of considering precritical deformation. Izvestiya Akademii Nauk SSSR, Otdelenie Tekhnicheskikh Nauk, Mekhanika i Mashinostroenie 4, 133–139, in Russian.

Axelrad, E.L., 1980. Flexible shells. In: Proceedings 15th IUTAM Congress, Toronto, pp. 45–56.

Axelrad, E.L., 1987. Theory of Flexible Shells. North-Holland, Amsterdam, The Netherlands.

Axelrad, E.L., Emmerling, F.A., 1983. Finite bending and collapse of elastic pressurized tubes. Ingenieur-Archiv 53, 41–52, in German.

Axelrad, E.L., Emmerling, F.A., 1984. Elastic tubes. Applied Mechanics Reviews 37 (7), 891–897.

Bathe, K.-J., Almeida, C.A., 1980. A simple and effective pipe elbow element. Journal of Applied Mechanics, ASME 47, 93–100.

Beskin, L., 1945. Bending of thin curved tubes. Journal of Applied Mechanics, ASME 67, A–1.

Boyle, J.T., 1981. The finite bending of curved pipes. International Journal of Solids and Structures 17, 515–529.

Brazier, L.G., 1927. On the flexure of thin cylindrical shells and other ''thin sections''. Proceedings of the Royal Society, Series A 116, 104–114.

Brush, D.O., Almroth, B.O., 1975. Buckling of Bars, Plates, and Shells. McGraw-Hill, New York.

Calladine, C.R., 1983. Theory of Shell Structures. Cambridge University Press, Cambridge, UK.

Clark, R.A., Reissner, E., 1951. Bending of curved tubes. Advances in Applied Mechanics 2, 93–122.

Chen, Y.N., Kempner, J., 1976. Buckling of oval cylindrical shells under compression and asymmetric bending. AIAA Journal 14, 1235–1240.
Cheng, D.H., Thailer, H.J., 1970. On bending of curved circular tubes. Journal of Engineering for Industry, ASME 9, 1175–1179.
Corona, E., Kyriakides, S., 1988. On the collapse of inelastic tubes under combined bending and pressure. International Journal of Solids and Structures 24, 505–535.
Crisfield, M.A., 1983. An arc-length method including line searches and accelerations. International Journal for Numerical Methods in Engineering 19, 1269–1289.
Emmerling, F.A., 1981. Nichtlineare Biegung eines schwach gekrummten Rohres. Zeitschrift fuer Angewandte Mathematik und Mechanik 61, T86–T89, in German.
Emmerling, F.A., 1982. Nichtlineare Biegung und Beulen von Zylindern und krummen Rohren bei Normaldruck. Ingenieur-Archives 52, 1–16, in German.
Fabian, O., 1977. Collapse of cylindrical, elastic tubes under combined bending, pressure and axial loads. International Journal of Solids and Structures 13, 1257–1270.
Gellin, S., 1980. The plastic buckling of long cylindrical shells under pure bending. International Journal of Solids and Structures 10, 397–407.
Gross, N., 1952. Experiments on short-radius pipe-bends. Proceedings of the Institution of Mechanical Engineers B 1, 465–479.
Gross, N., Ford, H., 1952. The flexibility of short-radius pipe-bends. Proceedings of the Institution of Mechanical Engineers B 1, 480–491.
Hutchinson, J.W., 1968. Buckling and initial postbuckling behavior of oval cylindrical shells under axial compression. Journal of Applied Mechanics, ASME 35, 66–72.
Ju, G.T., Kyriakides, S., 1992. Bifurcation and localization instabilities in cylindrical shells under bending II: Predictions. International Journal of Solids and Structures 29, 1143–1171.
Karamanos, S.A., 2000. Stability of elastic tubes under in-plane bending. Internal Research Report, LMSM 01/00, University of Thessaly, Volos, Greece.
Karamanos, S.A., Tassoulas, J.L., 1991. Stability of inelastic tubes under external pressure and bending. Journal of Engineering Mechanics, ASCE 117 (12), 2845–2861.
Karamanos, S.A., Tassoulas, J.L., 1996a. Tubular members I: Stability analysis and preliminary results. Journal of Engineering Mechanics ASCE 122 (1), 64–71.
Karamanos, S.A., Tassoulas, J.L., 1996b. Tubular members II: Local buckling and experimental verification. Journal of Engineering Mechanics ASCE 122 (1), 72–78.
Kyriakides, S., Shaw, P.K., 1982. Response and stability of elastoplastic circular pipes under combined bending and external pressure. International Journal of Solids and Structures 18 (11), 957–973.
Pardue, T.E., Vigness, I., 1951. Properties of thin-walled curved tubes of short-bend radius. Transactions of the ASME 73, 77–87.
Reissner, E., 1959. On finite bending of pressurized tubes. Journal of Applied Mechanics, ASME 26, 386–392.
Reissner, E., 1961. On finite pure bending of cylindrical tubes. Osterr. Ingenieur Archives 15, 165–172.
Reissner, E., Weinitschke, H.J., 1963. Finite pure bending of circular cylindrical tubes. Quarterly of Applied Mathematics XX (4), 305–319.
Rodabaugh, E.C., George, H.H., 1957. Effect of internal pressure on the flexibility and stress intensification factors of curved pipe or welding elbows. Transactions of the ASME 79, 939–948.
Seide, P., Weingarten, V.I., 1961. On the buckling of circular cylindrical shells under pure bending. Journal of Applied Mechanics ASME 28, 112–116.
Shaw, P.K., Kyriakides, S., 1985. Inelastic analysis of thin-walled tubes under cyclic bending. International Journal of Solids and Structures 21 (11), 1073–1100.
Sobel, L.H., 1977. In-plane bending of elbows. Computers and Structures 7, 701–715.
Stephens, W.B., Starnes Jr., J.H., Almroth, B.O., 1975. Collapse of long cylindrical shells under combined bending and pressure loads. AIAA Journal 13 (1), 20–25.
Timoshenko, S., Gere, J.M., 1961. Theory of Elastic Stability, second ed. McGraw-Hill, New York.
Thurston, G.A., 1977. Critical bending moment of circular cylindrical tubes. Journal of Applied Mechanics, Transactions of the ASME, Series E 44, 173–175.
Vigness, I., 1943. Elastic properties of curved tubes. Transactions of the ASME 65, 105–120.
von Karman, Th., 1911. Uber die Formuanderung dunnwandiger Rohre. Zeit Des Vereines deutcher Ingenieure 55, 1889–1895, in German.
Wood, J.D., 1958. The flexure of a uniformly pressurized, circular, cylindrical shell. Journal of Applied Mechanics, ASME 25, 453–458.